Draft version November 20, 2009
Preprint typeset using LaTeX style emulateapj v. 08/22/09

arXiv:0911.4121v1 [astro-ph.GA] 20 Nov 2009

THE ACS NEARBY GALAXY SURVEY TREASURY IV. THE STAR FORMATION HISTORY OF NGC 2976

Benjamin F. Williams[1], Julianne J. Dalcanton[1], Adrienne Stilp[1], Karoline M. Gilbert[1], Rok Roškar[1], Anil C. Seth[2], Daniel Weisz[3], Andrew Dolphin[4], Stephanie M. Gogarten[1], Evan Skillman[3], Jon Holtzman[5]

Draft version November 20, 2009

ABSTRACT

We present resolved stellar photometry of NGC 2976 obtained with the Advanced Camera for Surveys (ACS) as part of the ACS Nearby Galaxy Survey Treasury (ANGST) program. The data cover the radial extent of the major axis of the disk out to 6 kpc, or ∼6 scale lengths. The outer disk was imaged to a depth of $M_{F606W} \sim 1$, and an inner field was imaged to the crowding limit at a depth of $M_{F606W} \sim -1$. Through detailed analysis and modeling of these CMDs we have reconstructed the star formation history of the stellar populations currently residing in these portions of the galaxy, finding similar ancient populations at all radii but significantly different young populations at increasing radii. In particular, outside of the well-measured break in the disk surface brightness profile, the age of the youngest population increases with distance from the galaxy center, suggesting that star formation is shutting down from the outside-in. We use our measured star formation history, along with H I surface density measurements, to reconstruct the surface density profile of the disk during previous epochs. Comparisons between the recovered star formation rates and reconstructed gas densities at previous epochs are consistent with star formation following the Schmidt law during the past 0.5 Gyrs, but with a drop in star formation efficiency at low gas densities, as seen in local galaxies at the present day. The current rate and gas density suggest that rapid star formation in NGC 2976 is currently in the process of ceasing from the outside-in due to gas depletion. This process of outer disk gas depletion and inner disk star formation was likely triggered by an interaction with the core of the M81 group $\gtrsim 1$ Gyr ago that stripped the gas from the galaxy halo and/or triggered gas inflow from the outer disk toward the galaxy center.

Subject headings: galaxies: individual (NGC-2976) — galaxies: stellar populations — galaxies: spiral — galaxies: evolution

1. INTRODUCTION

Bursts of star formation play a significant and important role in the evolution of galaxies, particularly at low masses, such as dwarf galaxies. Star formation histories (SFHs) of dwarfs in the Local Group show strong evidence for past or current bursts (Mateo 1998; Dohm-Palmer et al. 2002; Dolphin et al. 2005; Young et al. 2007; Cole et al. 2007). The SFHs of the non-tidal dwarfs in the M81 group are equally diverse (Weisz et al. 2008). Recent observations of the entire local volume within 11 Mpc also indicate that bursts are an essential mode of star formation in low mass galaxies (Lee et al. 2009). Furthermore, numerical simulations suggest that episodic bursts of star formation should be common in low-mass galaxies, as gas is expelled by supernovae and then falls back into the galaxy (e.g. Stinson et al. 2007).

While there is little question that bursts are important in the formation and evolution of low-mass galaxies, most of the stellar mass in dwarfs may not form in bursts. For example, several studies suggest that dwarf irregular galaxies have relatively constant star formation histories (Gallagher et al. 1984; Greggio et al. 1993). Even though bursts clearly occur, most recent measurements suggest they are responsible for the production of only about a quarter of the stellar mass in dwarfs (Lee et al. 2009). Recent studies of nearby low mass starbursts have also put constraints on their durations, suggesting they typically last 200–400 Myr (McQuinn et al. 2009), in agreement with results from numerical simulations.

Much of the recent progress made in our understanding of the role of star formation bursts in the evolution of low-mass galaxies is due to the availability of deep resolved stellar photometry from the *Hubble Space Telescope (HST)*. Using such deep photometry, it possible to study galaxies using techniques previously available only within the Local Group. Rather than inferring details of evolution from integrated properties such as scale length, color, or surface brightness, the star formation history (SFH) of the stars in the galaxy can be determined by fitting the distribution of stars in color-magnitude diagrams (CMDs) with model distributions determined from stellar evolution isochrones, (see e.g. Holtzman et al. 1999; Dolphin 2000a; Williams 2002; Dohm-Palmer et al. 2002; Harris & Zaritsky 2004; Dolphin et al. 2005, for Local Group examples).

Detailed measurements of SFHs can be compared to the results of numerical simulations, which now probe the properties of the stellar populations they produce, to shed light on the physical processes responsible for the

---

[1] Department of Astronomy, Box 351580, University of Washington, Seattle, WA 98195; ben@astro.washington.edu; jd@astro.washington.edu; stephanie@astro.washington.edu; roskar@astro.washington.edu

[2] CfA Fellow, Harvard-Smithsonian Center for Astrophysics, 60 Garden Street, Cambridge, MA 02138; aseth@cfa.harvard.edu

[3] Department of Astronomy, University of Minnesota, 116 Church St. SE, Minneapolis, MN 55455; dweisz@astro.umn.edu; skillman@astro.umn.edu

[4] Raytheon, 1151 E. Hermans Road, Tucson, AZ 85706; dolphin@raytheon.com

[5] Department of Astronomy, New Mexico State University, Box 30001, 1320 Frenger St., Las Cruces, NM 88003; holtz@nmsu.edu

morphological structures we observe. Such simulations are beginning to show the importance of galaxy interactions in the evolution of disks (Governato et al. 2007), of internal dynamical interactions in distributing stars of different ages throughout the disk (Roškar et al. 2008), and of galaxy mass, feedback and gas availability in the process of star formation (Stinson et al. 2007). However, the simulations that show the most detailed features do not yet include environmental effects and cover limited ranges of galaxy mass.

NGC 2976, which has $M_B = -17$, $W_{20} = 165$ km s^{-1}, $(m-M)_0 = 27.76 \pm 0.23$, $A_V = 0.23$, and a morphology of SAc pec, (Simon et al. 2003; Karachentsev et al. 2002; Schlegel et al. 1998), is an excellent specimen for studying the effects of bursts of star formation and environment on the evolution of low-mass galaxies. This peculiar low-mass disk galaxy lies on the outskirts of the M81 group, outside of the Yun et al. (1994) H I maps. The inner disk of the galaxy contains many young stars, has a sharp truncation edge (Simon et al. 2003), appears to have a barred potential (Spekkens & Sellwood 2007), and may be inside of a larger spheroidal halo (Bronkalla et al. 1992). The galaxy's gas content and ongoing star formation (Bigiel et al. 2008; Leroy et al. 2008) are affecting its morphology. In order to investigate this impact, as well as potential effects of the M81 group environment, we have performed a systematic study of the stellar populations as a function of galactocentric distance in this peculiar galaxy. Our results suggest NGC 2976 is undergoing a transition from a burst of star formation to a more quiescent state, and thus we have a unique opportunity to study the final stages of a common mode of star formation.

Herein we report the SFH, measured via CMD fitting, of several regions of NGC 2976. We look for trends with radius, analyzing regions of constant crowding and differential extinction. We show that the ancient population is consistent with being similar over all radii. However, the age of the young population appears to increase sharply with radius beyond the disk break. By reconstructing the past gas surface density profile, we show that such an abrupt change in the age distribution is likely to be due to the depletion of gas in the NGC 2976 outer disk, possibly caused by an interaction with the core of the M81 group.

The paper is organized as follows. Section 2 details our data acquisition and reduction techniques. Section 3 compares and contrasts the recovered SFHs of the different regions. Section 4 discusses and interprets potential explanations for the differences in a galaxy evolution context. Finally, section 5 summarizes our main conclusions. We assume $(m-M)_0 = 27.76 \pm 0.23$ (Karachentsev et al. 2002) for conversions of angular measurements to physical distances and an inclination angle i=64.5° (de Blok et al. 2008) for surface density measurements. We adopt a WMAP (Dunkley et al. 2009) cosmology for all conversions between time and redshift.

2. DATA ACQUISITION, REDUCTION, AND ANALYSIS

2.1. *Acquisition*

2.1.1. *Outer Disk Field*

From 2006-Dec-27 to 2007-Jan-10, we observed a field covering the inner part of the NGC 2976 disk located at R.A. (2000) =146.902554 (09:47:36.61), decl. (2000) = +67.85705 (+67:51:25.4) with a rotation angle PA_V3=51.35. We also observed a field in the outskirts of the NGC 2976 disk located at R.A. (2000) =146.820171 (09:47:17.21), decl. (2000) = +67.898886 (+67:53:55.99) with a rotation angle PA_V3=52.75, taking advantage of the lower stellar density to image this outer field more deeply. Figure 1 shows outlines of the field locations, which cover the nucleus of the galaxy and extend to 5.7′ (6 kpc at NGC 2976) along the major axis. This distance corresponds to ∼6 scale lengths (mean of inner and outer disk) using the measured scale length from the isophotes on our F814W ACS images of the inner disk. If the disk/halo components of NGC 2976 scale as they do with larger disk galaxies, such as M31 and M81, the disk population should dominate out to at least 6 scale lengths, suggesting that our deep field is mainly probing the outer disk population.

In the outer field, we obtained 1 orbit of exposures with the ACS (Ford et al. 1998) through the F475W (SDSS g' equivalent) filter, 7 full-orbit exposures through the F606W (wide V) filter, and 10 full-orbit exposures through the F814W (I equivalent) filter. These data totaled 2418 s, 18716 s and 27091 s of exposure time in F475W, F606W, and F814W, respectively. In the inner field, we observed for 2 orbits, obtaining 2 dithered exposures through the F475W (wide B), F606W (wide V), and F814W (I equivalent) filters. Deeper observations for this field would not have been efficient, as the inner regions of the galaxy are too crowded to resolve faint stars. However, we dithered to cover the ACS chip gap so that we did not miss any of the main body of the galaxy. These data totaled 1570 s and 1596 s and 1622 s of exposure time in F475W, F606W, and F814W, respectively. All routine image calibration, including bias corrections and flat-fielding, were performed by the *HST* pipeline, OPUS version 2006_6, CALACS version 4.6.1.

2.2. *Reduction*

Photometry and artificial star tests were made as part of the ANGST survey pipeline. What follows is a brief description of the technique; readers are referred to Dalcanton et al. (2009) for a fuller description.

We initially processed the images by running the `multidrizzle` task within PyRAF (Koekemoer et al. 2002), which was used only to flag the cosmic rays in the individual images and to produce a reference coordinate system for the photometry. Once the cosmic rays were flagged, the photometry was measured simultaneously for all of the objects in the uncombined images using the software package DOLPHOT 1.0 (Dolphin 2000b) including the ACS module. This package is optimized for measuring photometry of stars on ACS images using the well-characterized and stable point spread function (PSF), calculated with TinyTim.[6] The software fits the PSF to all of the stars in each individual frame to find PSF magnitudes. It then determines and applies the aperture correction for each image using the most isolated stars, corrects for the charge transfer efficiency of the ACS detector, combines the results from the individual exposures, and converts the measured count rates to the VEGAmag system.

---

[6] http://www.stsci.edu/software/tinytim/

The DOLPHOT output was then filtered to only allow objects classified as stars with signal-to-noise >6 in both filters. The list was further culled using sharpness ($|F606W_{sharp} + F814W_{sharp}| < 0.27$) and crowding ($F606W_{crowd} + F814W_{crowd} < 0.1$). The sharpness cut was chosen based on the distribution of values in the original catalog. The crowding parameter gives the difference between the magnitude of a star measured before and after subtracting the neighboring stars in the image. When this value is large, it suggests that the star's photometry was significantly affected by crowding, and we therefore exclude it from our catalog. We also considered quality cuts based on the χ values, but rejected them when a correlation was found between χ and the local background. Our final star catalogs for the fields contained 96787 and 248864 stars detected in both the F606W and F814W filters for the outer and inner fields, respectively. We detected 14142 and 112756 stars in the F475W and F814W filters in the outer and inner fields, respectively.

Finally, a series of 2 million artificial star tests were run on each field. Model PSF stars were added to the data covering the full range of color, magnitude, and position space measured in the stellar photometry and including test stars up to 1 magnitude fainter than the faintest measured stars. The photometry was then measured by DOLPHOT again to determine the likelihood that a star was recovered, and if so, the offsets between its true and measured color and magnitude.

2.3. *CMD Fitting*

We measured the star formation rate and metallicity as functions of age, using the MATCH package (Dolphin 2002). The entire observed CMD is fitted by populating the stellar evolution models of Girardi et al. (2002, with updated AGB models from Marigo et al. 2008) with a given initial mass function (IMF), finding the distance modulus, extinction, and linear combination of ages and metallicities that best fit the observed color and magnitude distribution (see details in Dolphin 2002). A full discussion of the choice of fitting software and stellar evolution models used for the ANGST project is given in Williams et al. (2009).

2.3.1. *Field Division*

As can be seen in Figure 2, NGC 2976 shows strong radial variations in its surface brightness, dust content, and current star formation rate. We therefore choose to analyze the galaxy in a series of annuli. While the outer disk field does not show signs of structure that would warrant the division of the field into subregions, the inner disk field clearly has a strong gradient in surface brightness. This gradient causes the photometric completeness and error statistics to vary significantly with position. Following the galaxy's isophotes, we divided the inner field into 3 regions, shown in Figure 2. The inner ellipse contains the crowding-limited, high surface brightness inner galaxy and completely covers the area interior to the known break in NGC 2976's surface brightness profile at a radius of ∼1.2 kpc (inner r_s ∼1.3 kpc, outer r_s ∼0.6 kpc; Simon et al. 2003). This area also contains most of the structured dust content according to the 24μ *Spitzer* image shown in Figure 3. The outer ellipse marks the transition from this inner region to the uncrowded outer portions of the field. These 2 ellipses delineate 3 regions in the inner field. Along with the outer field, the field edges designate 4 separate regions of the galaxy for analysis, which we labeled from the inside-out as INNER-1, INNER-2, INNER-3, and OUTER. INNER-1 contains the disk break and the dusty, crowded areas within. INNER-2 is outside the disk break and high dust content but still contains a high density of stars with significant crowding, and INNER-3 is outside of the crowding-limited area. There is significant overlap in the projected radii probed by the INNER-3 and OUTER regions. The corresponding CMDs are shown in Figure 4.

With our artificial star tests, we determined the 50% completeness magnitudes of our 4 regions, given in Table 1. We applied these magnitude cuts to the data fitted by MATCH.

2.4. *Fitting Parameters*

To model the full CMD, we must adopt values for the binary fraction, IMF slope, the area of the CMD to include in the fit, the approximate distance and mean extinction to the stars in the field, and the binning of the stellar evolution models in time and metallicity. Below we discuss how we chose these parameters and how the choices impact our results.

For fitting purposes, we assumed a binary fraction of 0.35 and a Salpeter (1955) IMF when populating the model isochrones. As has been shown by other studies using this technique (e.g., Williams et al. 2007; Barker et al. 2007), our choice of IMF does not affect the relative star formation rates in the SFH, since our data do not probe the main sequence at low masses, where the IMF differs from a single power law (e.g. Kroupa 2002). Once the fits are complete, we can normalize the output star formation rates to other IMFs whenever necessary.

We initially allowed the distance modulus to range from 27.6 to 28.0 and the extinction to range from $A_V = 0.0$ to $A_V = 0.4$ in the OUTER region and from $A_V = 0.0$ to $A_V = 1.2$ in the INNER regions. Within these ranges, we allowed MATCH to determine the systematic errors that result from small changes to these parameters and to optimize the overall CMD fit, even in the presence of localized deficiencies in the model isochrones. However, once these systematic uncertainties were characterized, we reran our fits with the distance for all fields fixed to the best-fit value for the deep OUTER data ($m-M_0$=27.75). The resulting SFHs were indistinguishable from those obtained when distance was left as a free parameter.

The obvious dust visible in our inner disk field suggests that a single foreground extinction value cannot properly account for the effects of dust in our CMDs. We have attempted to minimize the effects of this problem in two ways. First, we have divided the field into separate regions with differing amounts of dust (e.g., Figure 2). The radial variation in internal extinction is evident in the foreground extinction values measured for each region by MATCH, which drop from $A_V = 0.56 \pm 0.07$ within the INNER-1 regions to $A_V = 0.34 \pm 0.07$ and $A_V = 0.21 \pm 0.07$ within the INNER-2 and INNER-3 regions respectively. The preferred extinction falls even further in the OUTER region, down to $A_V = 0.10 \pm 0.04$, which is below the value in the Schlegel maps of Galactic extinction. This slight discrepancy corresponds to a color difference of ∼0.03 mag. Such a slight difference is less than the size of the color bins in our Hess diagrams (0.05 mag). This type of discrepancy emphasizes the importance of fitting the overall distance and extinction as free parameters in order to compensate for such small discrepancies between the data and the model isochrones.

Second, we performed two fits to each of the INNER regions. One fit included 0.8 mag of differential extinction for ages >100 Myr, and the other fit included no differential extinction for ages > 100 Myr. By default, MATCH includes an additional ∼0.5 mag of differential extinction for ages <100 Myr. We found that including differential extinction for ages >100 Myr decreased the fit quality for the INNER-2, INNER-3 , and OUTER regions. Therefore, we accepted the fits that included no differential extinction for ages > 100 Myr for the these regions. For the INNER-1 region, we accepted only the fits with 0.8 mag of differential extinction. Including this amplitude of differential extinction improved the fit and brought the measured foreground extinction value to $A_V = 0.46 \pm 0.06$.

When fitting the CMD of the shallower and heavily reddened photometry of the INNER-1 region, we further limited the number of free parameters by imposing an "increasing metallicity" constraint on the fit, whereby the metallicity of the population was not allowed to decrease with time (within the measured errors). Without this constraint, the best-fitting SFH was found to be dominated by stars with solar metallicity at the oldest ages in order to fit the reddest and most heavily extincted red giants. Furthermore, without the constraint, the best-fit metallicity fluctuated from [M/H]=-0.6 to [M/H]=-0.1 then to [M/H]=-1.8 all in <1 Gyr. Imposing the metallicity constraint resulted in a lower fit quality, but it avoided unphysical solutions, such as order of magnitude fluctuations in metallicity on short ($\lesssim$ 100 Myr) timescales. With the constraint in place, the best-fitting metallicity for the young population was found to be -0.12±0.14 and stayed constant for the past Gyr. The effects of the constraint on the recent SFH are shown in Figure 5. The results with and without the constraint agree within the uncertainties for all but two 0.1 dex time bins. Thus, the metallicity constraint yielded a more physically plausible metallicity (with no wild fluctuations) while having minimal impact on the results of the age distribution of the young population. This lack of sensitivity to the metallicity constraint is likely due to the fact that the color of young stars on the upper main sequence are not very sensitive to metallicity.

For all regions, we initially used a fine logarithmic time and metallicity resolution (0.1 dex) to allow the best possible fit to the data. The resulting fit to our deep OUTER field is shown in Figure 6. While the overall fit to the CMD is quite good (upper panels), there are significant discrepancies in the red clump (overpopulated by the models) and brighter AGB bump (underpopulated by the models; see lower panels). Current isochrone models are not able to perfectly reproduce these features, which is a well-known deficiency of the isochrone set (Williams et al. 2009). After performing the full CMD fit, we binned the results to coarser time resolution to reduce our SFH uncertainties and to avoid drawing conclusions based on details that could be affected by deficiencies in the models or could not reliably be constrained by the data (see discussion in §4 of Williams et al. 2009, and §2.4.2 below).

2.4.1. *Uncertainty Estimates*

The SFHs shown in Figures 7-10 are subject to a number of uncertainties. These include both systematic uncertainties due to distance, extinction, and deficiencies in the model isochrones, as well as random errors due to the limited number of stars sampling the CMD features and the quality of the photometry. Estimates of the systematic uncertainties in color and magnitude in the models are automatically calculated by MATCH, which assesses the fit quality for a range of distance and extinction values. This process simulates uncertainties in the models, which are the systematic uncertainties in color and magnitude. We estimate the amplitude of the random uncertainties by generating 100 CMDs by randomly drawing stars from our observed CMD, allowing each bin in the Hess diagram to be populated according to a Poisson distribution, and measuring SFHs for the resulting CMDs. We adopted the standard deviation of these SFHs as our the random SFH errors for each subfield. These errors were then added in quadrature to the systematic errors determined by MATCH from fits using the range of possible distance and reddening values. The total gives our final uncertainties on the rate, metallicity, and cumulative fraction of stars formed as a function of time. We note that while these uncertainties completely describe the quality of the data, they do not account for covariance between adjacent time bins (Holtzman et al. 2007) and cannot quantify unknown uncertainties, such as evolutionary phase lifetimes, in the models.

2.4.2. *Assessing Temporal Resolution*

We have chosen time bin widths to reflect our sensitivity to age. To measure this sensitivity, we developed an iterative procedure to adjust the time bins included in the fit. Our initial fits to the CMDs use fine time bins of 0.1 dex. We then test the sensitivity to each of these 0.1 dex bins by removing each one and refitting the data. If a bin could be removed without significantly reducing the quality of the fit, we did not include it as a single bin in the final SFH, and we combined the bin with adjacent bins. We then iteratively removed adjacent 0.1 dex bins from the fitting until the quality of the fit was significantly worse. We define a significantly worse fit using the distribution of fit values from our Monte Carlo test runs. We calculate the standard deviation of this distribution, and we consider a fit values more than one standard deviation away from the best fit to be significantly worse.

However, this technique was biased against time bins that may truly contain no star formation, since such bins can never have an impact on the CMD regardless of their duration. Therefore if we found a time bin (or set of adjacent time bins) whose exclusion from the fit did not significantly change the fit quality, but that was surrounded by time bins whose exclusion from the fit did significantly change the fit quality, we allowed the time bin to remain independent, as a possible quiescent period in the SFH. For example, consider 3 adjacent time bins A, B, and C, and assume the exclusion of time bin B had no significant impact on the fit. If the exclusion of bin A negatively affected the fit and the exclusion of bin C also degraded the fit, then we infer that B is within a time period that is well-sampled in the CMD. In such a case, we do not merge bin B with bin A or bin C, even though B may not contain any star formation. In this way, we allow bins to contain no star formation.

The results of our time bin determination tests were qualitatively what would be expected. For the shallowest photometry of the INNER-1 region, we have only two statistically meaningful age bins for all stars >300 Myr. With the dust and crowding problems in this portion of the galaxy, the He-burning sequences blend with the RGB at $M_{F814W} \sim -3$, which corresponds to ages of $\sim$200 Myr. Furthermore, with the overlapping features and spread in RGB color from both the large photometry errors from crowding and significant internal extinction, the detailed age distribution of older stars from the RGB should not be reliable, as indeed our time bin tests reveal.

For the less crowded and less dusty regions of the INNER field, we found that we could use 2 age bins for ages >2 Gyr (2–10 Gyr and 10–14 Gyr). The independence of these two bins may be due to variations in the ratio of AGB to RGB stars and the slope of the RGB. A younger RGB (<10 Gyr) is slightly bluer, has a slightly steeper slope and a higher AGB/RGB ratio than an older RGB (>10 Gyr).

For the deep OUTER photometry, there is more information encoded in the CMD due to the presence of the older stellar populations that dominate the red clump. These features provide additional constraints on the SFR and allow shorter bin divisions at ages >1 Gyr.

The uncertainties in the derived metallicities tend to be largest at young ages (<100 Myr), where the only metallicity information comes from the short-lived He-burning sequences. These features tend to contain a relatively small number of stars, and the effects of metallicity on these features is not well understood in stellar evolution models (e.g. Maeder & Meynet 2000; Gallart et al. 2005; Przybilla et al. 2009).

Overall we are able to obtain very reliable estimates of the relative contributions of stars of old (>10 Gyr), intermediate (2–10 Gyr), and young (<1 Gyr) ages despite unavoidable sources of uncertainty. We likewise have reliable metallicities covering all but the youngest ages and high time resolution at young ages ($\lesssim$ 300 Myr). The cumulative age distribution is particularly stable against the uncertainties at intermediate ages, because the star formation rates in adjacent time bins are typically anticorrelated such that some fraction of the star formation will move back and forth between adjacent bins depending on small changes in the overall solution. Therefore we plot the cumulative distribution at the full resolution of the CMD fit.

3. RESULTS

The SFHs of all of our regions are shown in Figures 7-10. We first describe the most notable features of the results for each region, before discussing the integrated evolution of the galaxy in § 4.

3.1. *The SFH of OUTER*

The outer disk of NGC 2976 appears to be dominated by an old ($\gtrsim$ 8 Gyr), intermediate-metallicity (-0.5 $\lesssim$ [M/H] $\lesssim$ -1 -0.5) population, much like other outer disks, thick disks, and inner halos of ellipticals (e.g., see summary figure in Williams et al. 2009). About 60% of its outer disk stars were formed by $z \sim 1$ (see Figure 10). This age is consistent with the mean age of the M33 outer disk (Barker et al. 2007), which has a similar mass (V$_c \sim$ 110 km s^{-1} vs. V$_c \sim$ 85 km s^{-1} for NGC 2976).

While the SFH of the outer disk of NGC 2976 is consistent with roughly constant star formation over much of the age of the universe, in the last Gyr there has been a significant decline. Indeed, its recent star formation rate has been more than a factor of 5 lower than average for the past $\sim$800 Myr and more than a factor of 50 lower than average over the past $\sim$300 Myr. No areas of current star formation are apparent in the GALEX UV image (Gil de Paz et al. 2007) or in deep Hα images from SINGS (Kennicutt et al. 2003), which is consistent with our measurements. In fact, the mean age of the stars formed in the past Gyr is 740±150 Myr, and no stars younger than 130 Myr are required to produce an acceptable fit to the observed CMD (as determined by the statistical time bin tests described in § 2.4.2).

Although there are few young stars present in the outer disk, there is some question as to their origin. These stars may have formed *in situ*, or they may have scattered from the inner disk. If they formed in the outer disk, they may show some signs of clustering. However, as we show in Figure 11, where we plot the spatial distribution of upper main-sequence stars in this field (defined as $24 < F814W < 26$ and $-0.25 < F606W - F814W < 0.05$, or equivalently $5\,M_\odot \lesssim M \lesssim 12\,M_\odot$), these young stars are not found in clusters outside of the inner disk (seen in the lower-left edge of Figure 11). The youngest stars appear smoothly distributed. A 2-d Kolmogorov-Smirnov does not show a significant difference between the distributions of the upper main sequence stars and the red giants in the OUTER field (only 74% probability that the parent distributions are different).

We believe that the most plausible origin for the youngest stars we observe in these outer regions is that they were born in very small clusters that dissolved on short timescales. Typical small clusters with low star formation efficiency dissolve on timescales $\ll$100 Myr (Lada & Lada 2003), easily short enough to account for the few young stars we observe. However, we cannot conclusively determine if their birth clusters were within the outer disk. Lower-mass stars formed in the same clusters may still be present, but cannot be uniquely identified as young unlike the upper main sequence plotted in Figure 11.

As somewhat less plausible alternatives, the lack of current star formation or clustering of the few massive young stars ($\lesssim$ 300 Myr) in the outer disk is also consistent with the possibility that the young stars were not formed in the outer disk at all, but instead were scattered there from supernova kicks (e.g., Hoogerwerf et al. 2001) or interactions with the large number of star forming regions in the inner disk (Roškar et al. 2008). If these stars migrated the $\sim$2 kpc from the INNER-2 region in 130 Myr, their mean outward velocity would have been ∼14 km s^{-1}. Comparable mean outward velocities are seen in disk formation simulations, which show stars rapidly moving from circular orbits in the inner disk to circular orbits in the outer disk (Roškar et al. 2008).

3.2. *The SFH of the INNER Regions*

With the shallower photometry of the inner regions, we cannot reliably probe the detailed age distribution of the ancient populations, because the red giant branch alone can be equally well-fit by multiple combinations of ages and metallicities when there is no constraint on the fit from fainter CMD features, such as the red clump. This problem is often known as age-metallicity degeneracy, which is difficult to break with such shallow photometry. However, we still have ample information on SFRs during the past Gyr, which populates the luminous main sequence and He burning sequences. We therefore will focus most of our discussion of the inner regions on the recent SFH.

Although in the discussion below we present results for the F606W-F814W filter combination, we note that we have independently verified the recent SFHs (<500 Myr; <300 Myr for the INNER-1 region) using the F475W-F814W CMDs. In all 3 cases, the SFHs measured from the F475W-F814W CMDs were consistent with those measured from the F606W-F814W CMDs in this age range.

3.2.1. *The SFH of INNER-3*

Like the OUTER region, the SFH of this field shows no evidence for significant recent star formation. This consistency is not surprising, as there is substantial overlap in the projected radii of stars in these regions (see Table 1). After 400 Myr ago, there is a dramatic decrease in the star formation rate. The mean age of the stars formed in the past Gyr is 484±58 Myr, and no stars younger than 100 Myr are required to produce an acceptable fit to the observed CMD, as determined by the statistical time bin tests described in § 2.4.2.

Together, the star formation shutoff times and the mean ages of the young populations in OUTER and INNER-3 hint that we may be measuring a difference in the populations of these regions. However, this difference turns out to be attributable to the different depths of photometry in the two regions. When we remeasure the SFH of the OUTER region without including the photometry of stars fainter than F814W=26.8, the same cutoff used when fitting the INNER-3 data, the measurement of the mean age of the stars formed in the past Gyr drops somewhat to 580±130 Myr and the age of the youngest stars required to fit the CMD drops to 100 Myr. This test suggests that INNER-3 and OUTER contain similar populations; however, our INNER-3 photometry lacks the depth necessary to determine if there is a significant age difference between the young populations of the 2 regions.

Although we do not have very reliable measurements of the old populations in this regions, we note that our fits suggest the age distribution prior to the steep drop in star formation is consistent with being constant from ∼1–10 Gyr, although variations on shorter timescales are certainly allowed by the data, given the large width of our time bins in this region. The age and metallicity distribution of the old stars in this region appears comparable to that of all the regions studied, including the much deeper OUTER region.

3.2.2. *The SFH of INNER-2*

This region shows only a small decline in star formation ∼200 Myr ago. Unlike the complete truncation of star formation seen in INNER-3 and OUTER, stars have continued to form at this radius, albeit at a reduced rate. The mean age of the stars formed in the past Gyr is somewhat younger than that of the INNER-3 region (394±42 Myr), and the youngest stars required to fit the CMD are also younger (13 Myr). This age difference is consistent with that inferred from visual inspection of the CMDs of INNER-2, which has a much more pronounced main sequence than that seen in INNER-3 (see Figure 4). Furthermore, it is consistent with the truncation of star formation from the outside-in.

Furthermore, the old population appears again similar to those of the other regions. This similarity of the ancient populations across such a large radial extent may indicate that the older population is more well-mixed than the younger population, as would be expected given the relatively short dynamical time for the galaxy (∼180 Myr) and current barred kinematics (Spekkens & Sellwood 2007). While the continuous exponential surface brightness profile may favor a pure stellar disk, one could also interpret the difference between the old and young populations as being two kinematically distinct components of the galaxy. There indeed have been previous claims that NGC 2976 consists of a young disk and an old spheroidal halo (Bronkalla et al. 1992), and the consistency of our measurements of the older populations across NGC 2976 likewise supports those claims. Kinematic tests would be required to verify this scenario, however.

3.2.3. *The SFH of INNER-1*

The SFH of the innermost region is the most difficult to constrain due to its high crowding, bright completeness limit, and significant differential extinction. These effects cause confusion in the CMD at magnitudes as bright as F606W∼24. These limitations reduce the reliability of the age distribution for ages $\gtrsim$ 300 Myr ago and remove any constraint on the SFH prior to 3 Gyr ago. However, the mean age of the stars formed in the past Gyr in this region is 360±30 Myr, again younger than those of the other regions. In addition, the youngest stars necessary to fit the CMD are 6 Myr. These results show that the age of the youngest stars and the mean age of the stars formed in the past Gyr increase monotonically with galactocentric distance (see Figure 12). Together, all of the data are consistent with the truncation of star formation from the outside-in.

4. DISCUSSION: THE RECENT SFH OF NGC 2976

NGC 2976 does not look like any other nearby galaxy. Its bright inner disk has little organized structure and a sharp truncation edge. The atypical appearance of NGC 2976 could indicate that this galaxy is in the midst of a short-lived and interesting time in its evolution. The recent shutdown of star formation seen in the SFHs of the outer regions of the disk is also consistent with the possibility that NGC 2976 is undergoing a metamorphosis. To gain additional insight into this process, we studied the recent SFHs of our 4 regions in more detail, including detailed comparisons with the galaxy's kinematics and gas content.

The recent SFHs of our 4 regions are shown with 0.1 dex time resolution in Figure 8. Although these small time bins are finer than the sensitivity of the data (shown in Figure 7), we include it to ease comparisons with our analysis of the gas consumption below. There is clearly a lack of recent star formation in the outer regions as compared with the inner regions, which we interpret as a shutdown of star formation from the outside-in. This shutdown appears to have begun in the outer disk ∼0.5–1 Gyr ago. There is also an increase in the age of the young (<1 Gyr) stars with galactocentric distance, shown in Figure 12, consistent with this interpretation. We return to the origin of this shutdown in § 4.2 below.

4.1. *Timescales*

The evolution of the star formation in NGC 2976 could be related to a number of different timescales in the galaxy, including the dynamical timescale, the time since the last interaction with M81, and/or the gas consumption lifetime in the disk. These timescales are provided in Table 2.

We estimate the dynamical time using the H I rotation curve of de Blok et al. (2008). NGC 2976 has a rotation velocity of $\sim$85 km s^{-1} at 2.5 kpc (∼2 inner disk scale lengths), giving it a dynamical timescale of ∼180 Myr, somewhat shorter than the apparent star formation truncation timescale.

The time since the last interaction with M81 is not well-constrained, but can be estimated by making some reasonable assumptions. Even though NGC 2976 lies outside the core of the group, the H I structure of the group suggests that NGC 2976 has had recent interactions with the galaxies in the core of the M81 group (M81, M82, and NGC 3077 Yun 1999; Appleton et al. 1981). Likewise, its tidal index is elevated (Θ=2.7; Karachentsev et al. 2004), also consistent with recent interactions. Assuming that the relative velocity of NGC 2976 and M81 is not more than the velocity dispersion of the group (110 km s^{-1}; Huchra & Geller 1982) and that their relative measured distances in the ANGST survey (3.57 Mpc for NGC 2976 and 3.58 Mpc for M81, Dalcanton et al. 2009) are correct, then any close passage was at least 1.3 Gyr ago assuming an angular separation of 148 kpc. Our SFHs do not detect any burst in activity near that age limit. However, a passage close to our lower time limit could have potentially stripped the halo gas and/or induced the radial inflow of gas from the outer disk, causing subsequent star formation to truncate from the outside-in (see §4.3).

The gas consumption timescale of the INNER-1 region is comparable to the truncation timescale we see in our SFHs. From the THINGS H I map (Walter et al. 2008), the current mean gas density (assuming $\Sigma_{\rm gas}$=1.45 × $\Sigma_{\rm HI}$) of the NGC 2976 inner disk is ∼10 $M_\odot$ pc^{-2} out to 90″ (r∼1.6 kpc), beyond which it rapidly declines to the noise level ($\Sigma_{\rm HI}$ ∼ 1.5 $M_\odot$ pc^{-2}) by 200″ (r∼3.5 kpc). Our SFH gives a current star formation rate density in the innermost region of ∼0.036 $M_\odot$ yr^{-1} kpc^{-2}, yielding a gas consumption lifetime of ∼280 Myr in the inner disk. If we were to normalize our rates to a Kroupa (2002) IMF, the SFRs would be a factor of ∼1.5 lower, making the gas consumption lifetime closer to ∼0.6 Gyr. In either case, these timescales are similar to that at which the star formation is measured to be shutting down.

The gas consumption lifetime of the INNER-2 region (∼2.6 Gyr) is considerably longer than that of the INNER-1 region. This longer lifetime reflects the lower star formation rate we have measured for this region. While star formation in this region has apparently slowed down, it has not yet ceased.

Outside of the INNER-2 region, the gas is of very low surface density (∼1.7 $M_\odot$ pc^{-2}), well below the canonical Kennicutt (1989) star formation threshold. As may therefore be expected, we measure only an upper-limit on star formation in the most recent epoch ($<8\times10^{-6}$ $M_\odot$ yr^{-1} kpc^{-2} in the 4–10 Myr bin), which yields a gas consumption lifetime greater than a Hubble time. Even if we consider the higher mean rate back to 80 Myr (2.5×10^{-5} $M_\odot$ yr^{-1} kpc^{-2}), the gas consumption lifetime is still greater than a Hubble time, indicating that significant star formation has effectively ceased in the outer disk.

4.2. *Gas Content*

The consistency between the gas consumption timescale and the star formation truncation timescale of the inner disk suggests that gas consumption has played a key role in the recent evolution of NGC 2976. To further investigate this possibility, we performed a study of the correlation between gas density and star formation in the disk of NGC 2976 over the past several hundred Myr. We assume that all of the stars that formed during a given time interval must have been in the form of gas at the beginning of that time interval. When this gas is added to the gas seen at the present day, we can infer the gas density in the recent past, and then compare it to the subsequent star formation rate. We can do this at increasing lookback times, giving us a way of probing the correlation between gas and star formation rate at a range of epochs, but at a single location within the disk.

We begin with the present day gas density measurements from THINGS data, assuming that $\Sigma_{gas} = 1.45\Sigma_{\rm HI}$. We then assume that all stars formed from a previously-existing gas disk that was in place at the beginning of each time interval. Our method therefore requires that the gas disk had a higher surface density in the past in order to provide the material for all of the star formation that subsequently occurred.

We limit our estimates to the times for which we have the most reliable SFHs in all regions (<500 Myr ago). We also make a correction for stellar evolution, which returns some fraction of the new stellar mass back into the interstellar medium, such that a given mass of new stars consumes a somewhat smaller net mass of gas. We assume that stellar evolution quickly recycles 20% of the mass of stellar mass back to the gas phase. This fraction corresponds to all stars >8 $M_\odot$ (assuming a Kroupa IMF integrated from 0.1 $M_\odot$ to 100 $M_\odot$), which return their mass to the ISM on timescales shorter than 100 Myr. The exact value of this fraction had minimal impact on our estimates.

Applying our SFH measurements to the current gas surface density at different galactocentric distances yields a reconstruction of the gas surface density profile over the past 450 Myr (Figure 13). The inferred gas density profile ∼450 Myr ago appears to approach that of a single exponential with a scale length of ∼0.7 kpc, or ∼40″, similar to the scale length of the outer stellar disk (34″; Simon et al. 2003). If our assumptions of little gas infall or outflow over the past ∼450 Myr are correct, then the gas profile of NGC 2976 had this simpler, single exponential form in the past. The gas density of ∼50 $M_\odot$ pc^{-2} inferred for the inner disk 450 Myr ago is very high for a galaxy of this mass (typically $\lesssim$ 10 $M_\odot$ pc^{-2} Swaters et al. 2002), suggesting that there may have been radial inflow of gas from the outer disk $\gtrsim$ 500 Myr ago.

The very high gas density 450 Myr ago led to a very high star formation rate, and rapid consumption of the gas. Indeed, the regions inside the disk break have converted ∼75% of the gas present ∼500 Myr ago into stars, indicating very rapid gas depletion at recent times. In contrast, the low surface density regions beyond the disk break have converted only $\lesssim$ 30% of the gas present ∼500 Myr ago into stars.

The rapid decrease in the gas surface density dramatically dropped the gas mass fraction of the galaxy. To determine the gas fraction in the disk as a function of galactocentric distance and time, we started with the present-day stellar density from the K-band profile of Simon et al. (2003), assuming M/L_K=1.1 (obtained by correcting Bell et al. (2003) to a true Salpeter (1955) IMF to agree with our SFH calculations). Our estimate of the current total gas mass fraction (∼0.19 out to 3.5 kpc) agrees within 10% of those of Leroy et al. (2008) obtained from *Spitzer* and THINGS (∼0.17). The estimated gas fraction at previous epochs changes much more drastically in the inner regions than in the outer regions. While the gas fraction has stayed relatively constant at ∼0.26 for the past ∼500 Myr in the outer disk, the gas fraction of the inner disk has plummeted from ∼0.30 to ∼0.07. These values could be indicative of a massive old stellar population recently augmented by a long ($\gtrsim$ 500 Myr) burst of star formation that is now in the process of ending. Our measurements of the gas fraction at previous epochs (back to 500 Myr ago) are consistent with the large range observed by Geha et al. (2006) for galaxies of similar baryonic mass, suggesting that individual galaxies can likely cycle throughout the observed range in response to gas infall, redistribution, and consumption.

Our inferred gas densities at previous epochs also allowed us to study the historical relationship between average gas density and average star formation rate density at different radii in the recent past. Figure 14 shows the historical relationship between gas density and star formation rate for the INNER-1 (black) and INNER-2 (gray) regions. The gas density values are the same as those shown in the left panel of Figure 13, and the corresponding star formation rates are those from our SFH measurements averaged over the same epochs. Although the axes of this plot are interrelated (i.e. the cumulative SFH was used to derive the horizontal axis), the relationship between the differential SFH and the cumulative SFH is not required to be a power law.

The dotted line in Figure 14 marks the Schmidt law in the form

$$\frac{\Sigma_{SFR}}{\mathrm{M_\odot\ yr^{-1}\ kpc^{-2}}} = a(\frac{\Sigma_{gas}}{10\ \mathrm{M_\odot\ pc^{-2}}})^N.$$

We show the relation found in THINGS for $\Sigma_{H\ I}$ in NGC 2976 (log(a)=-1.88; N=1.78, Bigiel et al. 2008). Their gas densities were determined using the same H I data used here, but their SFRs were determined from a combination of GALEX FUV and Spitzer 24μm maps and considered only star formation visible at the present day. Their observed relation was thus based on many regions within the same galaxy, but only at the present day.

Figure 14 shows that the historical star formation rates at the range of gas densities shown in Figure 13 are generally consistent with the present day relationship seen by THINGS. Therefore the relation measured using a range of SFRs and H I densities from different *locations* in the disk is consistent with our values for SFRs and H I densities from different *times* in the history of the disk. The consistency suggests that our main assumption (the gas was in place ∼500 Myr ago) is likely to be correct. If so, any gas infall and/or inflow responsible for the high gas densities during that epoch must have occurred prior to 500 Myr ago, when NGC 2976 may have been significantly closer to the core of the M81 group.

The observed change in star formation efficiency at low gas densities (seen as a change of slope in Figure 14) is common in nearby galaxies. Many of the galaxies in THINGS sample show a steeper relation at gas densities $\lesssim$ 10 $M_\odot$ pc^{-2} than at higher densities. The results from the INNER-2 region show a very steep relation. This region, which lies just outside the disk break, therefore has likely experienced a significant drop in star formation efficiency recently, as its gas surface density dropped below ∼7 $M_\odot$ pc^{-2}. This sharp drop in star formation efficiency at low surface densities is even steeper than that found by THINGS for NGC 2976.

Finally, we use the relation between gas density and star formation rate in NGC 2976 measured by Bigiel et al. (2008) for gas densities below 10 $M_\odot$ pc^{-2} to predict the future gas and stellar mass profiles. Assuming all of the stellar mass that forms depletes the gas reservoir, we calculate the radial profile of the gas and stars for future epochs and plot them in Figure 13. The stellar mass profile is expected to undergo very little change, and the gas continues to be depleted while maintaining the shape of its density profile. Overall, much less dramatic evolution is seen in the future prediction than in the past reconstruction, which is again consistent with NGC 2976 being at the end of a burst of star formation.

4.3. *Comparisons with Simulations*

The young stellar component of NGC 2976 appears to be confined to a disk. Although the disk has relatively chaotic structure and a sharp break, there is only limited evidence that processes and structures similar to those we observe in NGC 2976 exist in current simulations of disk formation and evolution.

In simulations of dwarf disks, Stinson et al. (2009) have identified a mechanism by which the gas disk shrinks over time due to the depletion of gas in the central portions of the disk, which reduces the amount of available pressure support. As the gas disk shrinks, star formation recedes from the outside-in, in qualitative agreement with our results for NGC 2976. In their simulations, the process occurs over longer timescales (∼Gyrs); however, their simulations are for somewhat smaller disks than NGC 2976, do not include interactions, and show that the timescale of the process decreases as the mass of the disk increases.

On the other hand, in simulations of larger disks, Roškar et al. (2008) have shown that radial scattering can lead to a reversal of the disk age gradient outside of the disk break. This effect also produces a gradient in the age of the youngest stars, as it takes longer for stars to be scattered to larger radii. This gradient in the age of the youngest stars is comparable to what we have observed in NGC 2976. However, the timescale is again longer than that observed in NGC 2976 (>1 Gyr predicted vs. <1 Gyr observed).

To understand the recent evolution of NGC 2976, comparisons with simulations and observations of interacting galaxies may be more appropriate. It is possible that NGC 2976's recent interaction with the core of the M81 group caused internal gas redistribution due to tidal forces and/or an episode of halo gas stripping. Either of these processes can lead to a shutdown of star formation from the outside-in.

The strong tidal forces within an interaction could cause a major redistribution of gas within NGC 2976, such that gas from the outer disk funnels to the inner disk, increasing the central star formation rate at the expense of the outer disk. The central metallicities of interacting galaxies strongly suggest that such radial gas inflow occurs in such interactions (Kewley et al 2006). Hydrodynamical simulations are in general agreement with the observations (e.g., Iono et al. 2004). The central gas surface densities inferred for previous epochs for NGC 2976 (§ 4.2; ~ 50 M$_\odot$ pc^{-2}) are much higher than those typically seen in Irr galaxies of similar luminosity to NGC 2976 ($\lesssim 10$ M$_\odot$ pc^{-2}; Swaters et al. 2002). It is possible that much of this gas fell into the central regions from the outer disk prior to 500 Myr ago, when NGC 2976 was closer to the core of the M81 group.

An interaction with the galaxy group could also result in the stripping of gas from the NGC 2976 halo. Numerical simulations of galaxy groups have recently shown evidence that when halo gas is lost from disks due to ram pressure stripping, the proceeding truncation of star formation then occurs from the outside-in. The timescale for such truncation due to strangulation is $\lesssim 0.5$ Gyr (Bekki 2009) and is shorter for less massive galaxies. These simulations are therefore consistent with what we observe in NGC 2976. Either or both of these interaction scenarios (inflow or stripping) would be consistent with the recent gas consumption in NGC 2976 as well as simulations of disk galaxies in group environments.

5. CONCLUSIONS

We have measured resolved stellar photometry of 2 HST/ACS fields covering ∼6 scale lengths of the NGC 2976 disk. The resulting color-magnitude diagrams show a radial trend where the fraction of main sequence stars decreases with increasing radius, even outside of the most active central region. Modeling the CMDs to recover the age distribution of the stars reveals that, while the outer regions have undergone very little star formation for the past ∼500 Myr, the inner regions have continuously formed stars to the present. We see this lack of young stars begin at a radius of ∼3 kpc, well outside of the disk break. Inside of 3 kpc, the recent star formation rate is similar to the rate in past epochs. This trend of increasing age of young stars with galactocentric distance is similar to an age trend recently measured in the disk of the Large Magellanic Cloud, also using CMD analysis (Gallart et al. 2008). The trend suggests a truncation of star formation from the outside-in.

The radially-dependent differences in the young populations are in contrast to the apparent uniformity of the old populations across the galaxy, which appear to be consistent with one another in proportion and metallicity. It is possible that the old stars are dominated by a spheroidal component of the galaxy (Bronkalla et al. 1992) and only the young stars are truly sampling the disk. Alternatively, the old stars may simply be a well-mixed old disk population. Given the correct barred potential of the galaxy (Spekkens & Sellwood 2007), radial orbits should have led to significant radial redistribution of stars.

Detailed study of the gas in NGC 2976 shows clear evidence that it has recently been rapidly depleted. The current gas densities and gas consumption lifetimes in NGC 2976 suggest that the dominant mechanism behind the observed age gradient is the quenching of the gas disk. The lack of clustering of the few young stars at large radii does admit the possibility that radial scattering may have played a role in placing some of the young stars into the outer disk. However, we consider the shutting down of star formation in the disk from the outside-in to be the dominant process in the current morphological transition occurring in NGC 2976. This process may be related to ram pressure stripping of the halo gas and/or internal gas redistribution induced by tidal forces due to the most recent interaction with the core of the M81 group.

We thank Gregory Stinson for helping to compare the dwarf simulations to our measurements. Support for this work was provided by NASA through grant GO-10915 from the Space Telescope Science Institute, which is operated by the Association of Universities for Research in Astronomy, Incorporated, under NASA contract NAS5-26555.

REFERENCES

Appleton, P. N., Davies, R. D., & Stephenson, R. J. 1981, MNRAS, 195, 327

Barker, M. K., Sarajedini, A., Geisler, D., Harding, P., & Schommer, R. 2007, AJ, 133, 1138

Bekki, K. 2009, ArXiv e-prints, 0907.4409

Bell, E. F., McIntosh, D. H., Katz, N., & Weinberg, M. D. 2003, ApJS, 149, 289

Bigiel, F., Leroy, A., Walter, F., Brinks, E., de Blok, W. J. G., Madore, B., & Thornley, M. D. 2008, AJ, 136, 2846

Bronkalla, W., Notni, P., & Mutter, A. A.-R. 1992, Astronomische Nachrichten, 313, 1

Cole, A. A., et al. 2007, ApJ, 659, L17

Dalcanton, J. J., et al. 2009, ApJS, 183, 67

de Blok, W. J. G., Walter, F., Brinks, E., Trachternach, C., Oh, S.-H., & Kennicutt, R. C. 2008, AJ, 136, 2648

Dohm-Palmer, R. C., Skillman, E. D., Mateo, M., Saha, A., Dolphin, A., Tolstoy, E., Gallagher, J. S., & Cole, A. A. 2002, AJ, 123, 813

Dolphin, A. E. 2000a, ApJ, 531, 804

Dolphin, A. E. 2000b, PASP, 112, 1383

Dolphin, A. E. 2002, MNRAS, 332, 91

Dolphin, A. E., Weisz, D. R., Skillman, E. D., & Holtzman, J. A. 2005, ArXiv Astrophysics e-prints, astro-ph/0506430

Dunkley, J., et al. 2009, ApJS, 180, 306

Ford, H. C., et al. 1998, in Presented at the Society of Photo-Optical Instrumentation Engineers (SPIE) Conference, Vol. 3356, Proc. SPIE Vol. 3356, p. 234-248, Space Telescopes and Instruments V, Pierre Y. Bely; James B. Breckinridge; Eds., ed. P. Y. Bely & J. B. Breckinridge, 234

Gallagher, J. S., III, Hunter, D. A., & Tutukov, A. V. 1984, ApJ, 284, 544

Gallart, C., Stetson, P. B., Meschin, I. P., Pont, F., & Hardy, E. 2008, ApJ, 682, L89

Gallart, C., Zoccali, M., & Aparicio, A. 2005, ARA&A, 43, 387

Geha, M., Blanton, M. R., Masjedi, M., & West, A. A. 2006, ApJ, 653, 240

Gil de Paz, A., et al. 2007, ApJS, 173, 185

Girardi, L., Bertelli, G., Bressan, A., Chiosi, C., Groenewegen, M. A. T., Marigo, P., Salasnich, B., & Weiss, A. 2002, A&A, 391, 195

Governato, F., Willman, B., Mayer, L., Brooks, A., Stinson, G., Valenzuela, O., Wadsley, J., & Quinn, T. 2007, MNRAS, 374, 1479

Greggio, L., Marconi, G., Tosi, M., & Focardi, P. 1993, AJ, 105, 894

Harris, J., & Zaritsky, D. 2004, AJ, 127, 1531

Holtzman, J. A., Dalcanton, J. J., Garnett, D., Sarajedini, A., & Williams, B. F. 2007, AJ, submitted

Holtzman, J. A., et al. 1999, AJ, 118, 2262

Hoogerwerf, R., de Bruijne, J. H. J., & de Zeeuw, P. T. 2001, A&A, 365, 49

Huchra, J. P., & Geller, M. J. 1982, ApJ, 257, 423

Iono, D., Yun, M. S., & Mihos, J. C. 2004, ApJ, 616, 199

Karachentsev, I. D., et al. 2002, A&A, 383, 125

Karachentsev, I. D., Karachentseva, V. E., Huchtmeier, W. K., & Makarov, D. I. 2004, AJ, 127, 2031

Kennicutt, R. C., Jr. 1989, ApJ, 344, 685

Kennicutt, R. C., Jr., et al. 2003, PASP, 115, 928

Kewley, L. J., Geller, M. J., & Barton, E. J. 2006, AJ, 131, 2004

Koekemoer, A. M., Fruchter, A. S., Hook, R. N., & Hack, W. 2002, in The 2002 HST Calibration Workshop : Hubble after the Installation of the ACS and the NICMOS Cooling System, Proceedings of a Workshop held at the Space Telescope Science Institute, Baltimore, Maryland, October 17 and 18, 2002. Edited by Santiago Arribas, Anton Koekemoer, and Brad Whitmore. Baltimore, MD: Space Telescope Science Institute, 2002., p.337, ed. S. Arribas, A. Koekemoer, & B. Whitmore, 337

Kroupa, P. 2002, Science, 295, 82

Lada, C. J., & Lada, E. A. 2003, ARA&A, 41, 57

Lee, J. C., Kennicutt, R. C., José G. Funes, S. J., Sakai, S., & Akiyama, S. 2009, ApJ, 692, 1305

Leroy, A. K., Walter, F., Brinks, E., Bigiel, F., de Blok, W. J. G., Madore, B., & Thornley, M. D. 2008, AJ, 136, 2782

Maeder, A., & Meynet, G. 2000, ARA&A, 38, 143

Marigo, P., Girardi, L., Bressan, A., Groenewegen, M. A. T., Silva, L., & Granato, G. L. 2008, A&A, 482, 883

Mateo, M. L. 1998, ARA&A, 36, 435

McQuinn, K. B. W., Skillman, E. D., Cannon, J. M., Dalcanton, J. J., Dolphin, A., Stark, D., & Weisz, D. 2009, ApJ, 695, 561

Przybilla, N., Firnstein, M., & Nieva, M.-F. 2009, ArXiv e-prints

Roškar, R., Debattista, V. P., Stinson, G. S., Quinn, T. R., Kaufmann, T., & Wadsley, J. 2008, ApJ, 675, L65

Salpeter, E. E. 1955, ApJ, 121, 161

Schlegel, D. J., Finkbeiner, D. P., & Davis, M. 1998, ApJ, 500, 525

Simon, J. D., Bolatto, A. D., Leroy, A., & Blitz, L. 2003, ApJ, 596, 957

Spekkens, K., & Sellwood, J. A. 2007, ApJ, 664, 204

Stinson, G., Dalcanton, J., Quinn, T., Gogarten, S., Kaufmann, T., & Wadsley, J. 2009, ArXiv e-prints

Stinson, G. S., Dalcanton, J. J., Quinn, T., Kaufmann, T., & Wadsley, J. 2007, ApJ, 667, 170

Swaters, R. A., van Albada, T. S., van der Hulst, J. M., & Sancisi, R. 2002, A&A, 390, 829

Walter, F., Brinks, E., de Blok, W. J. G., Bigiel, F., Kennicutt, R. C., Thornley, M. D., & Leroy, A. 2008, AJ, 136, 2563

Weisz, D. R., Skillman, E. D., Cannon, J. M., Dolphin, A., Kennicutt, R. C., Jr., Lee, J., & Walter, F. 2008, ApJ, submitted

Williams, B. F. 2002, MNRAS, 331, 293

Williams, B. F., et al. 2007, ApJ, 656, 756

Williams, B. F., et al. 2009, AJ, 137, 419

Young, L. M., Skillman, E. D., Weisz, D. R., & Dolphin, A. E. 2007, ApJ, 659, 331

Yun, M. S. 1999, in IAU Symposium, Vol. 186, Galaxy Interactions at Low and High Redshift, ed. J. E. Barnes & D. B. Sanders, 81

Yun, M. S., Ho, P. T. P., & Lo, K. Y. 1994, Nature, 372, 530

TABLE 1
Properties of the Designated Regions

Region	R_{in} (kpc)[a]	R_{out} (kpc)	R_{med} (kpc)[b]	Stellar Mass Fraction[c]	$F475W_{50}$[d]	$F606W_{50}$[e]	$F814W_{50}$[f]
INNER-1	0	1.5	1.0	0.86	25.9	25.8	25.0
INNER-2	1.5	3.0	2.1	0.13	27.4	27.1	26.6
INNER-3	2.4	6.2	3.3	0.03	27.9	27.9	27.2
OUTER	2.4	8.2	3.7	0.03	27.7	28.9	28.2

[a] Deprojected radii. These overlap because the ellipticity of the isophotes used to define the regions were not precisely those expected for standard value for the inclination (64.5°) we assumed for the disk.

[b] The median galactocentric distance of the stars in the the region.

[c] The fraction of stellar mass contained between R_{in} and R_{out} assuming the profile shown in Figure 13.

[d] The 50% completeness limit of the F475W data.

[e] The 50% completeness limit of the F606W data.

[f] The 50% completeness limit of the F814W data.

TABLE 2
Relevant timescales for NGC 2976

Galaxy Process	Timescale in NGC 2976 (Gyr)
Dynamical (rotation)	0.18
Recent shutdown of star formation	$\sim$0.5
Gas Consumption of INNER-1	$\sim$0.35
Interaction with M81	$\gtrsim$ 1.3
Gas Consumption of INNER-2	$\sim$2.6
Gas Consumption of INNER-3	$\gtrsim$ 10

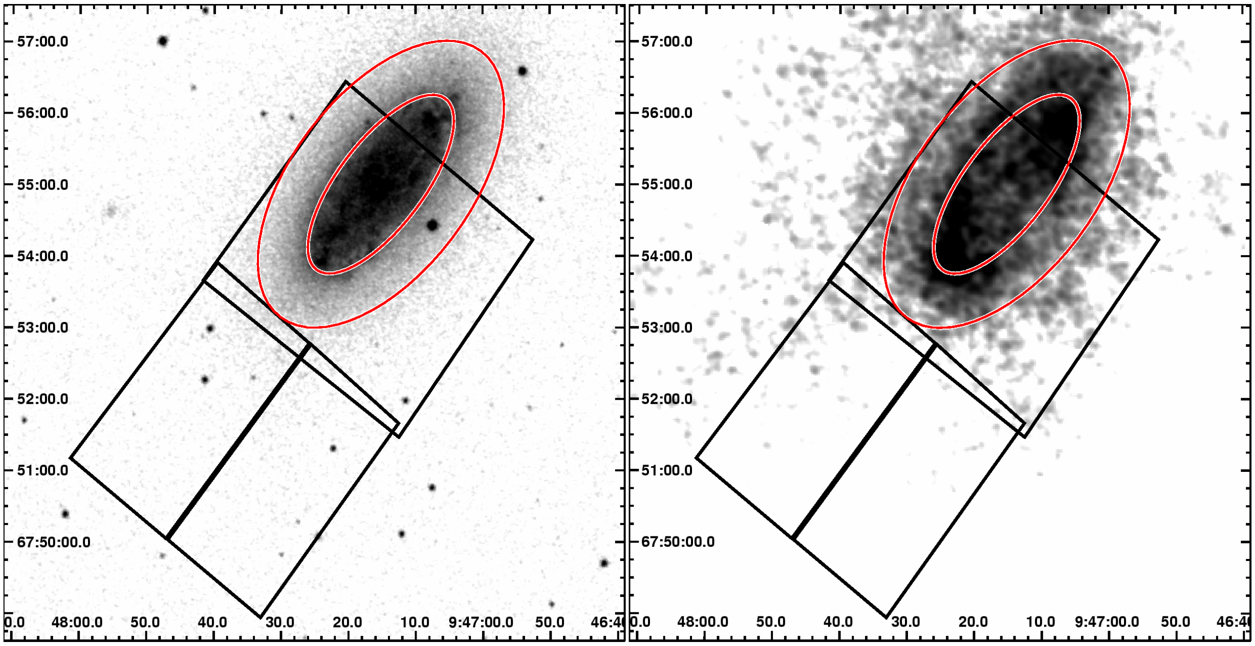

Fig. 1.— The locations of our NGC 2976 fields are shown on a DSS image (left) and the H I Nearby Galaxy Survey (THINGS) image (right). The inner field shows no chip gap because we dithered over the chip gap in this field. Ellipses denote our region boundaries (see § 2).

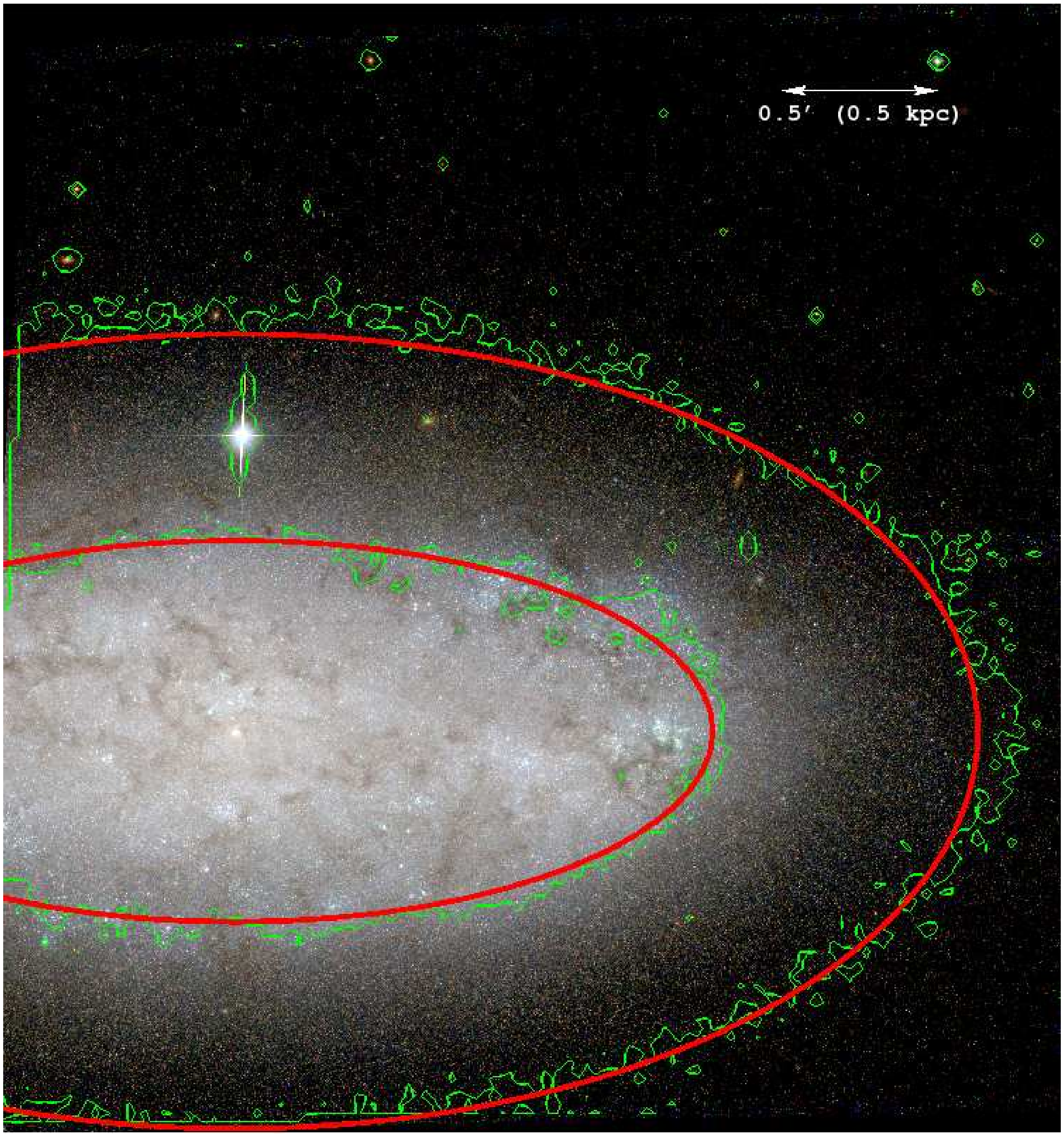

FIG. 2.— Our division of the inner field into 3 regions is shown (see § 2.3.1). Thin white lines show the contours of constant surface brightness. Thick white lines show the ellipses used to cleanly sort stars into their appropriate regions. The scale bar in the upper right corner shows 0.5′, or 0.5 kpc at the distance of NGC 2976. The ellipses are centered at R.A. (J2000) = 09:47:15.185, decl. (J2000) = +67:55:00.59, and they have semi-major axes of 90″ and 140″ and semi-minor axes of 36″ and 75″.

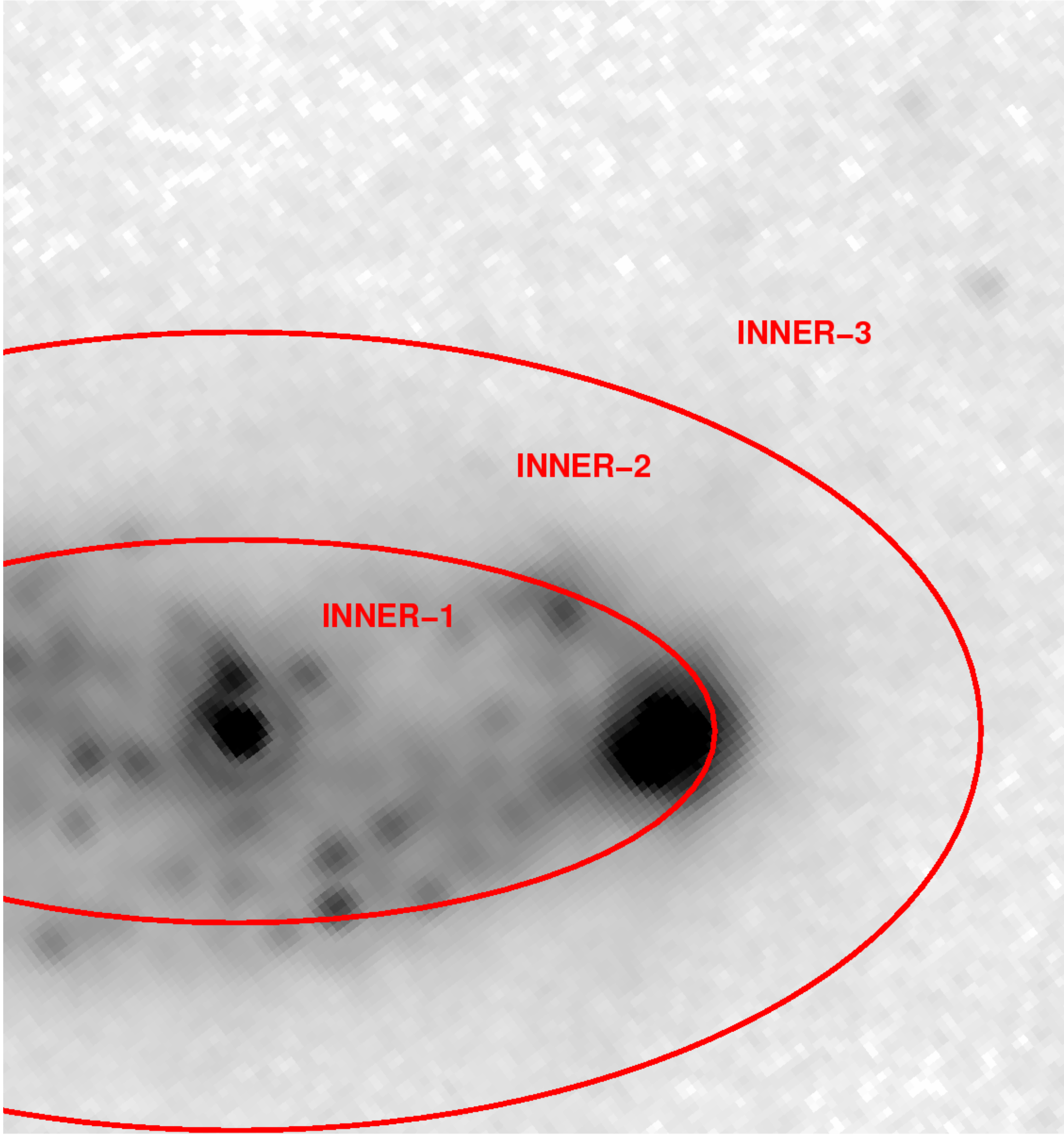

FIG. 3.— Our division of the galaxy marked with ellipses superimposed on a 24μm *Spitzer* image (same dimensions as in Figure 2). The star formation is confined to the inner ellipse (see § 2.3.1).

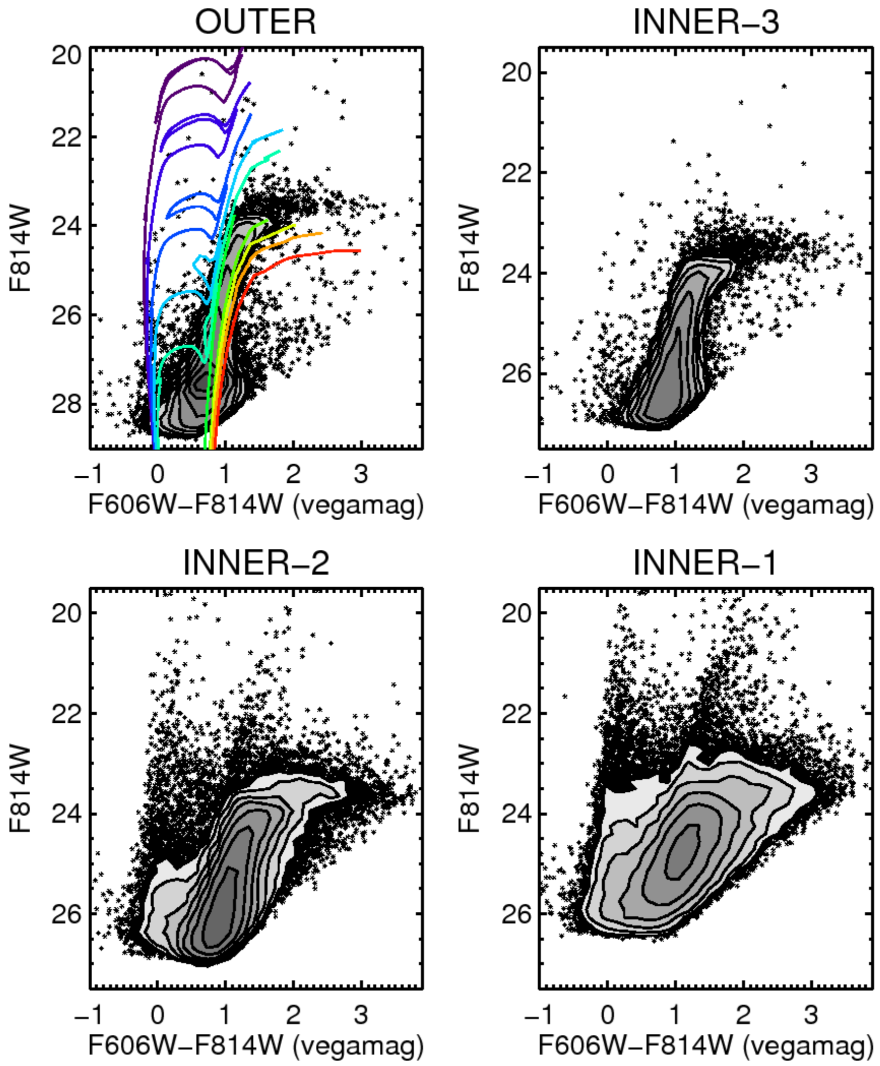

FIG. 4.— CMDs of the four regions (see § 2.3.1). Contours show the density of points where they would otherwise saturate the plot. Levels are 1, 2, 4, 8, 16, 32, 64, and 128 thousand points mag^{-2}. Lines in the upper-left panel show a small subset of isochrones for reference (Marigo et al. 2008, shifted assuming $A_V = 0.1$ and $(m - M)_0 = 27.75$). The 10 isochrones shown are (from blue to red): [M/H]=-0.4 and log(age) = 7.3,7.6,8.0,8.3,8.6, followed by log(age)=10.0 and [M/H] = -1.3,-0.7,-0.4,-0.2,0.0, respectively.

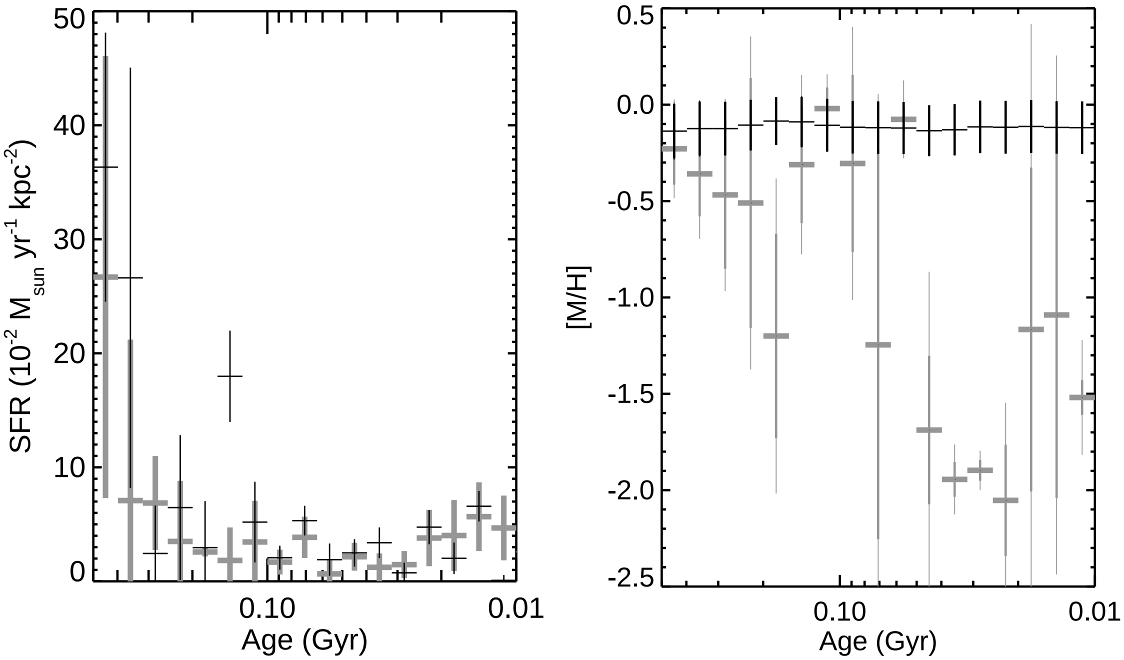

Fig. 5.— *Left:* The recent SFH for the INNER-1 region at full time resolution assuming metallicity stays constant or increases with time (thin black) and making no assumptions about enrichment (thick gray). The results agree within the uncertainties for all times except the 10-12.5 Myr and 125-160 Myr bins. *Right:* The recent metallicity history assuming metallicity stays constant or increases with time (thin black) and making no assumptions about enrichment (thick gray). Note that the age distribution is not strongly affected by the metallicity distribution at these ages (see § 2.3).

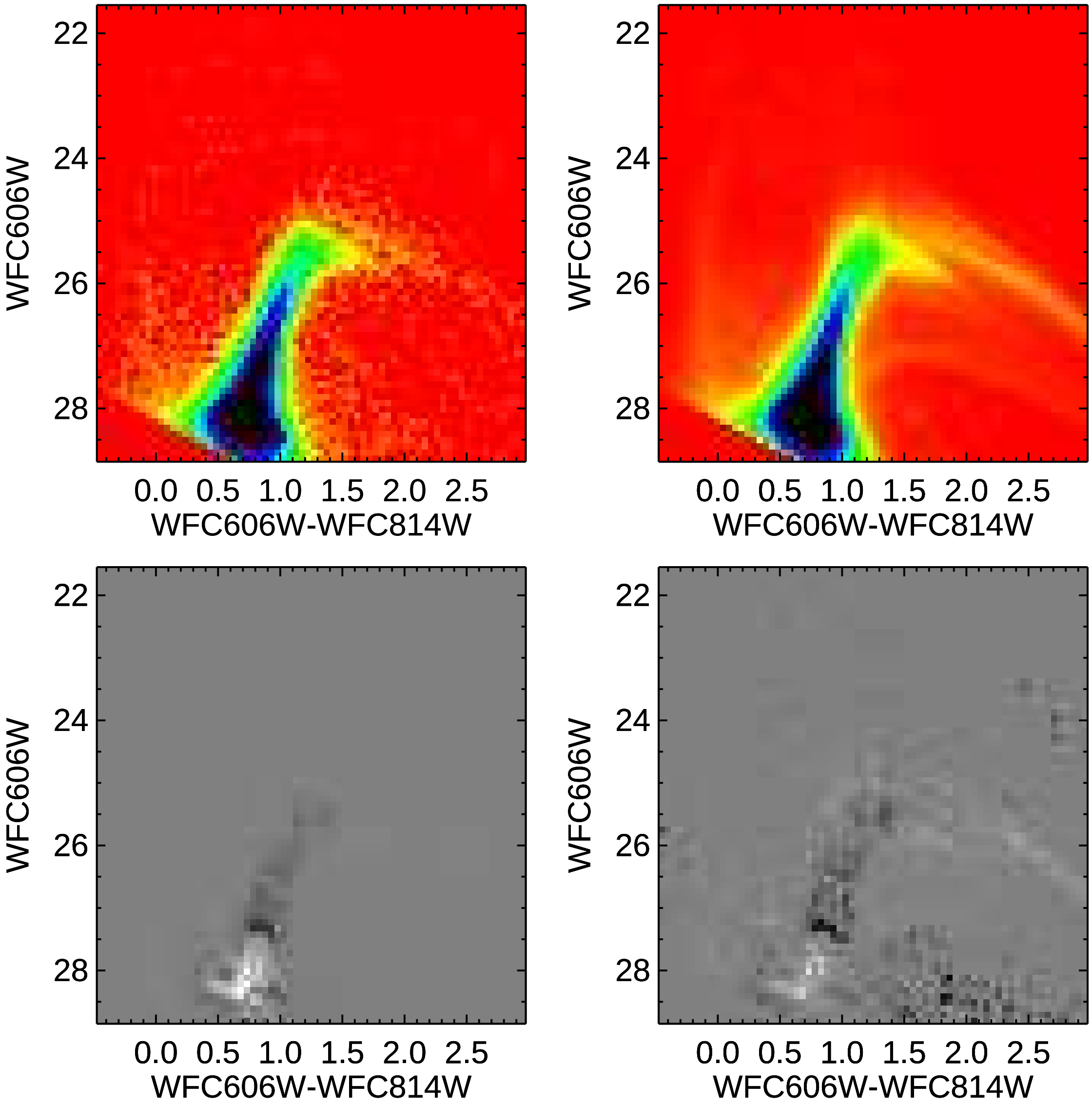

FIG. 6.— Our best full CMD fit to the data from the OUTER field (see § 2.3). *Upper-left:* The observed CMD. *Upper-right:* The best-fitting model CMD from MATCH. *Lower-left:* The residual CMD (data-model). The range plotted is from -163 to +109 stars bin^{-1} (lightest to darkest). *Lower-right:* The deviations shown in *lower-left* normalized by the Poisson error in each CMD bin. This plot shows the significance of the residuals in *lower-left*. The most significant residuals correspond to roughly -21% and 27% deviations (lightest to darkest) and occur at the locations of the red clump (F606W$\sim$28.3; overpopulated by the models) and AGB bump (F606W$\sim$27.3; underpopulated by the models), where the current models are known to suffer from deficiencies (Gallart et al. 2005).

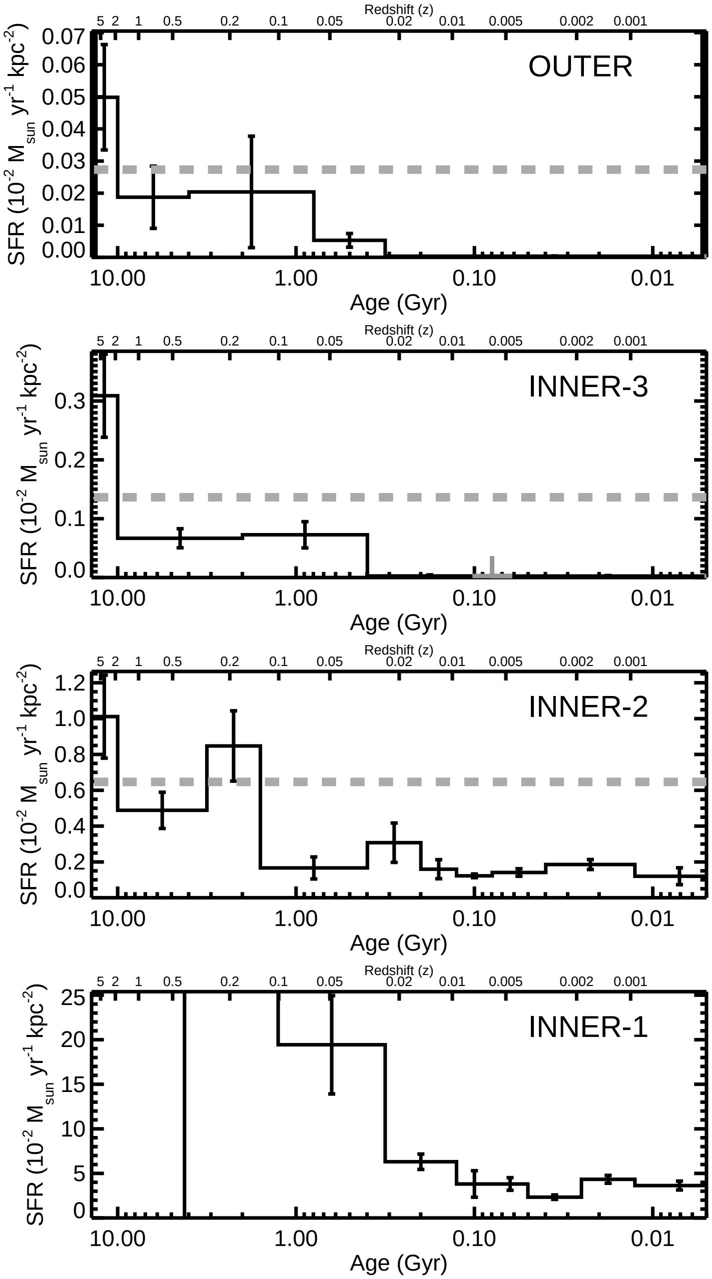

Fig. 7.— The SFH of the outermost (top) to innermost (bottom) regions (see § 2.4.2 and § 3). The solid histogram marks the star formation rate surface density as a function of time for the past 14 Gyr. The dashed line marks the mean rate. Edges of time bins with rates too low to see are marked with heavy gray ticks on the bottom axis. The outer 3 regions show star formation that declines to the present, with star formation truncating more than 300 Myr ago in the outermost field. The innermost field was too shallow to provide any constraint on the population older than 3 Gyr (error bar extends off the plot in both directions for the oldest time bin).

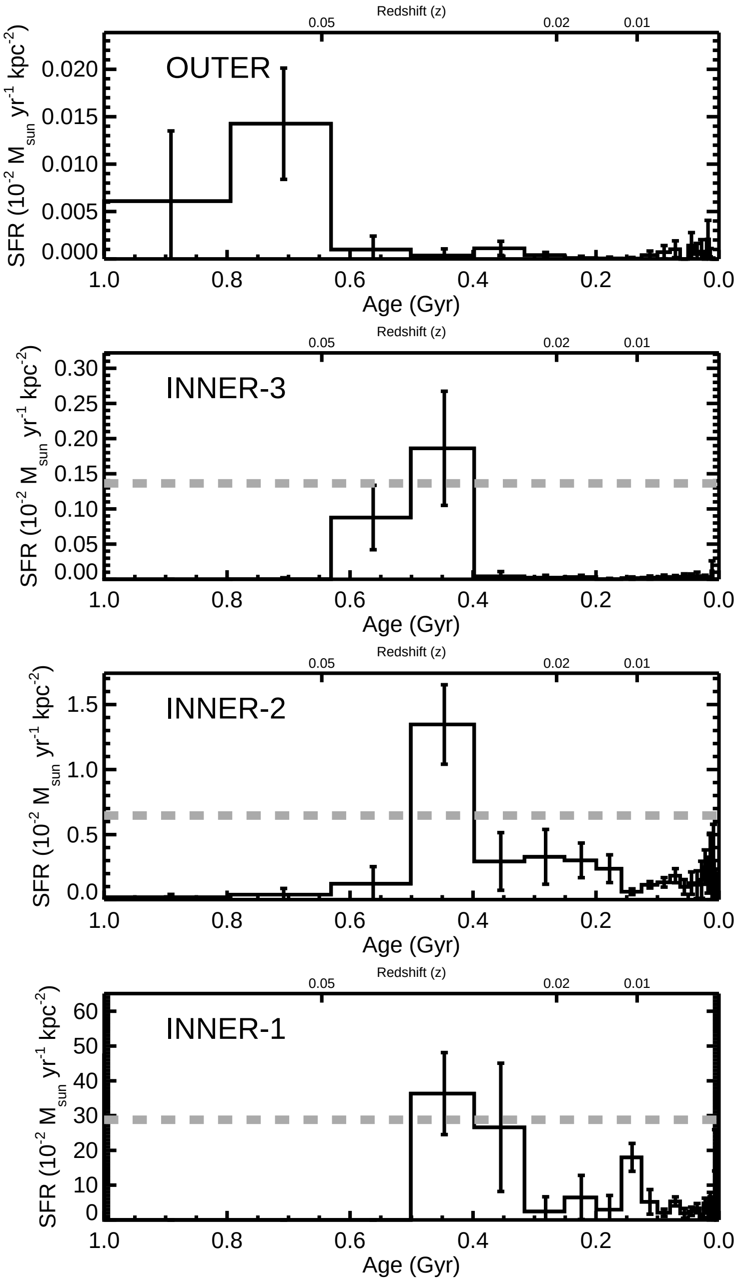

FIG. 8.— Recent SFHs for the 4 regions for the past Gyr plotted on a linear timescale at 0.1 dex time resolution (see § 4). Differences between these and Figure 7 reveal the effects of applying time resolution that is finer than the data can probe, as determined by our Monte Carlo tests (see § 2.4.2). The dashed line indicates the mean rate for the full history of the galaxy.

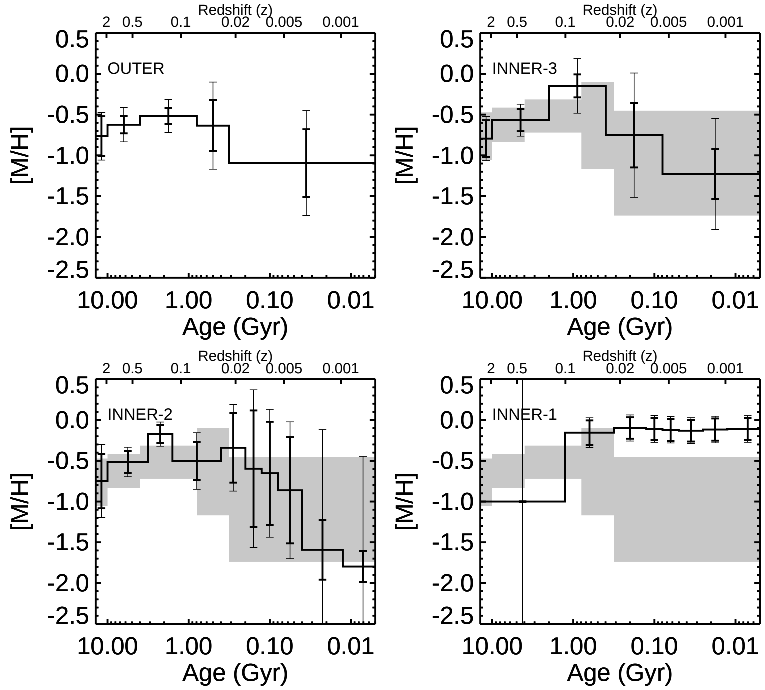

FIG. 9.— The mean metallicity and metallicity range of the population as a function of time for each of the regions (see § 3.1). Heavy bars mark the measured metallicity range, and lighter error bars mark how that range can slide because of uncertainties in the mean metallicity. There is little significant evidence for any evolution in metallicity, despite on-going star formation. Shaded regions show how the metallicity history measurement from our deepest data (OUTER) compares with the measurements from the shallower inner regions. Our data do not put tight constraints on the metallicity at young ages ($\lesssim$ 100 Myr). Errors are smaller and the mean metallicity is different for the innermost region because of our assumption of increasing metallicity with time when fitting these shallower data.

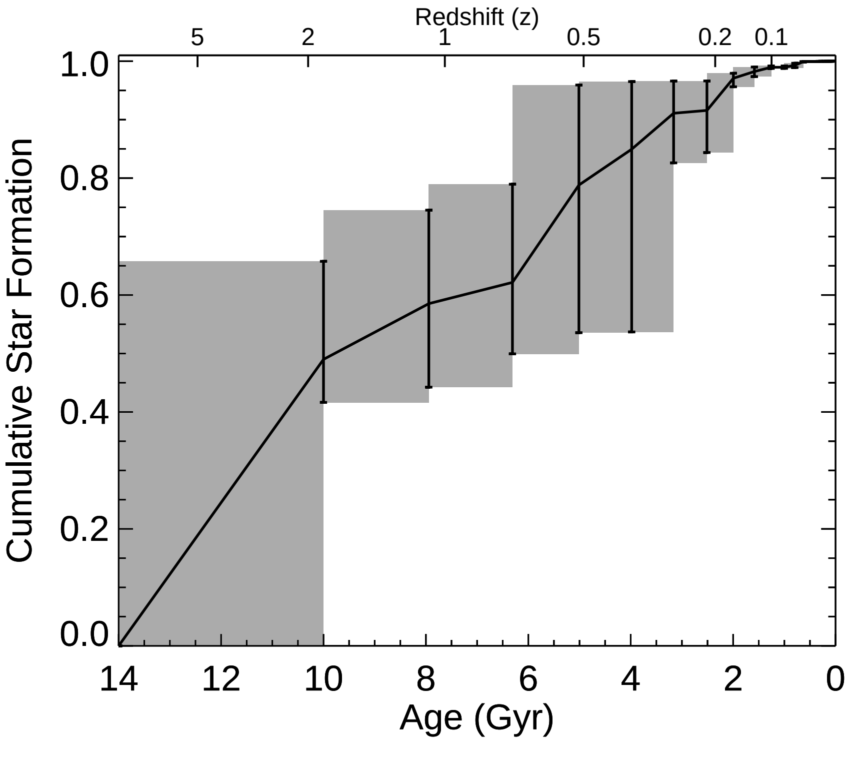

FIG. 10.— The normalized cumulative star formation of the OUTER field as determined by the MATCH package (see § 3.1). *Black Line:* the best fit, assuming constant star formation within each time bin. *Gray Regions:* the evolution allowed by the measured errors. Roughly 60% of the stellar mass was formed by $z = 1$.

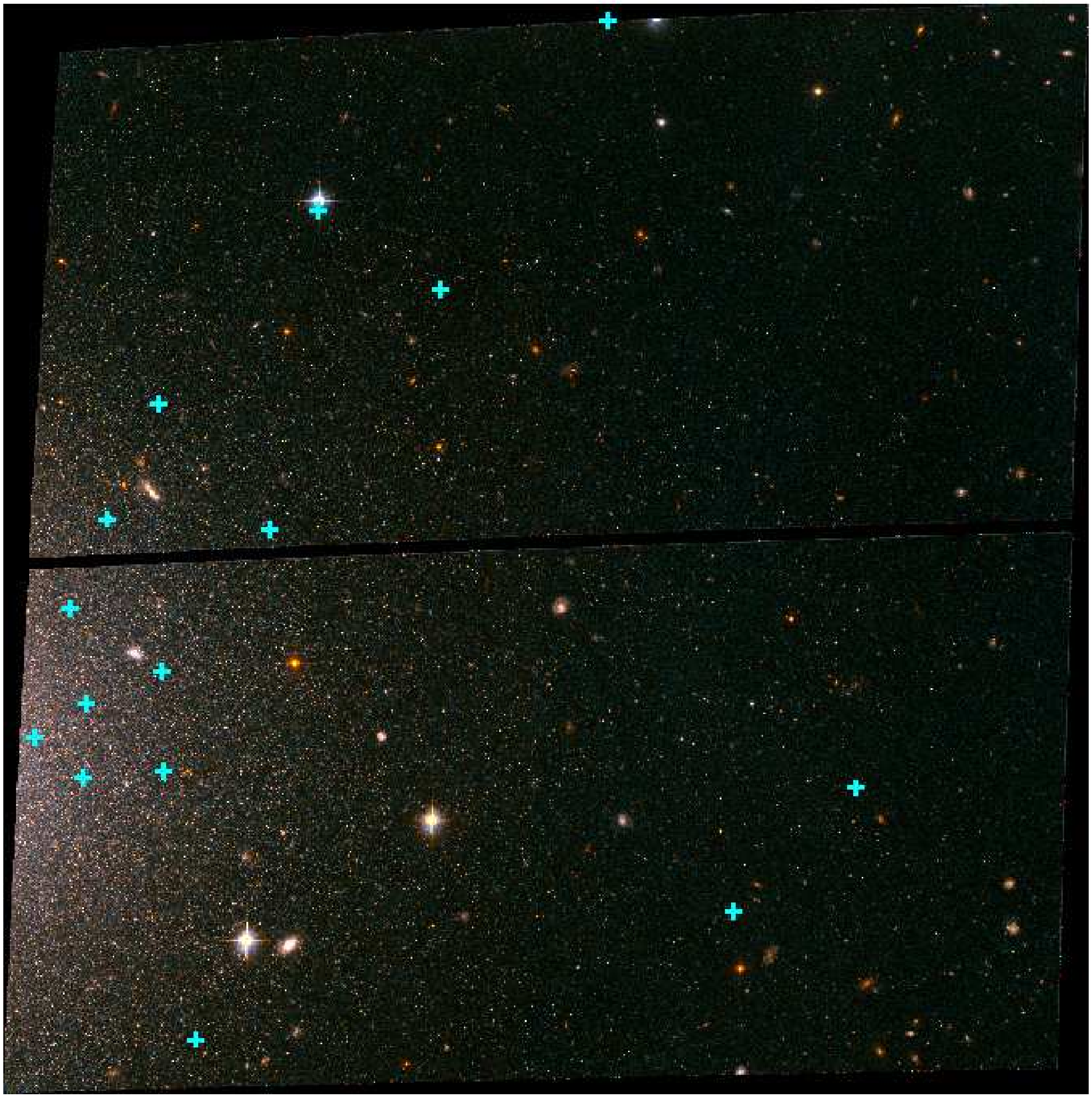

Fig. 11.— A color image of our DEEP outer field. Cyan crosses mark the locations of objects that fall on the upper main sequence in our CMDs. No clustering of the most massive young stars is detected in this portion of the outer disk according to a 2-d Kolmogorov-Smirnov test (see § 3.1). We verified that our quality cuts did not reject stars in clusters.

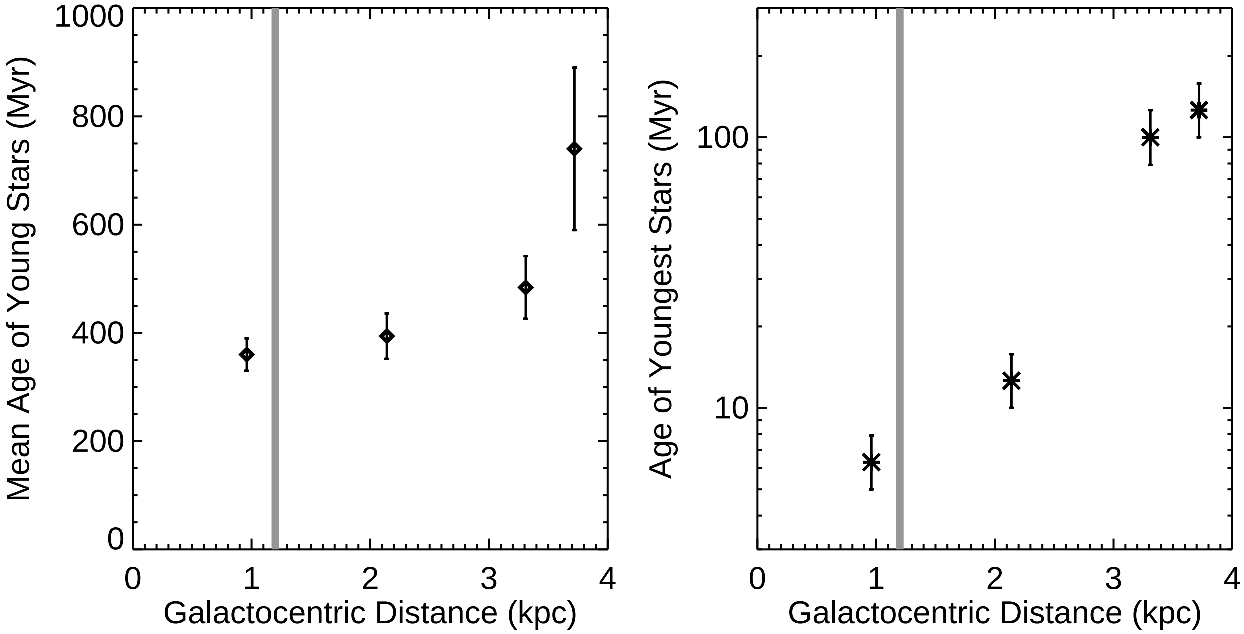

FIG. 12.— *Left:* The mean age of the stellar mass formed in the past Gyr as a function of median distance from the galaxy center. The age of the young stars increases with galactocentric distance. *Right:* The age of the youngest stars necessary to produce an acceptable fit to the CMD as a function of median distance from the galaxy center (see § 4). Errors mark our 0.1 dex time bins. *Gray vertical lines:* The location of the disk break. By both measurements, the age of the young stars increases monotonically with galactocentric distance.

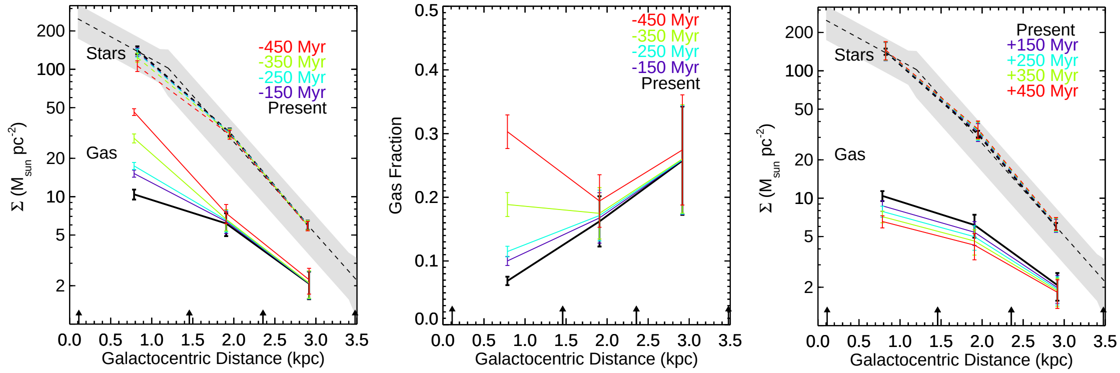

FIG. 13.— *Left: Solid Lines:* The gas surface density inferred for different epochs [150 Myr ago (blue), 250 Myr ago (cyan), 350 Myr ago (green), 450 Myr ago (red)], assuming that the stars formed in each epoch depleted an existing gas reservoir (see § 4.2). The current surface density of gas was measured from the THINGS data assuming a correction factor of 1.45 to convert from H I density to total gas density (black). *Dashed Lines:* The surface density of stars over the past 450 Myr. Colors mark the same epochs as for the gas. Present star density (shaded region) assumes and extrapolates the Simon et al. (2003) K-band profile and M/L_K=1.1, obtained by correcting Bell et al. (2003) to a true Salpeter (1955) IMF. Error bars shown are relative errors between the mass densities at different lookback times; these errors do not include the error in the original stellar mass profile. *Arrows:* Limits of the radial bins, as defined based on the SFH measurements and the regions with good H I data. *Middle:* The gas mass fractions in different radial bins for the same epochs as *Left*. *Right:* Same as *Left* but the gas densities plotted are anticipated for future epochs, assuming that the stars formed in each epoch will deplete the existing gas reservoir [150 Myr (blue), 250 Myr (cyan), 350 Myr (green), 450 Myr (red)]. Overall, the predicted profiles do not change as significantly as the reconstructed ones shown in *Left* indicating that the burst of star formation is ending.

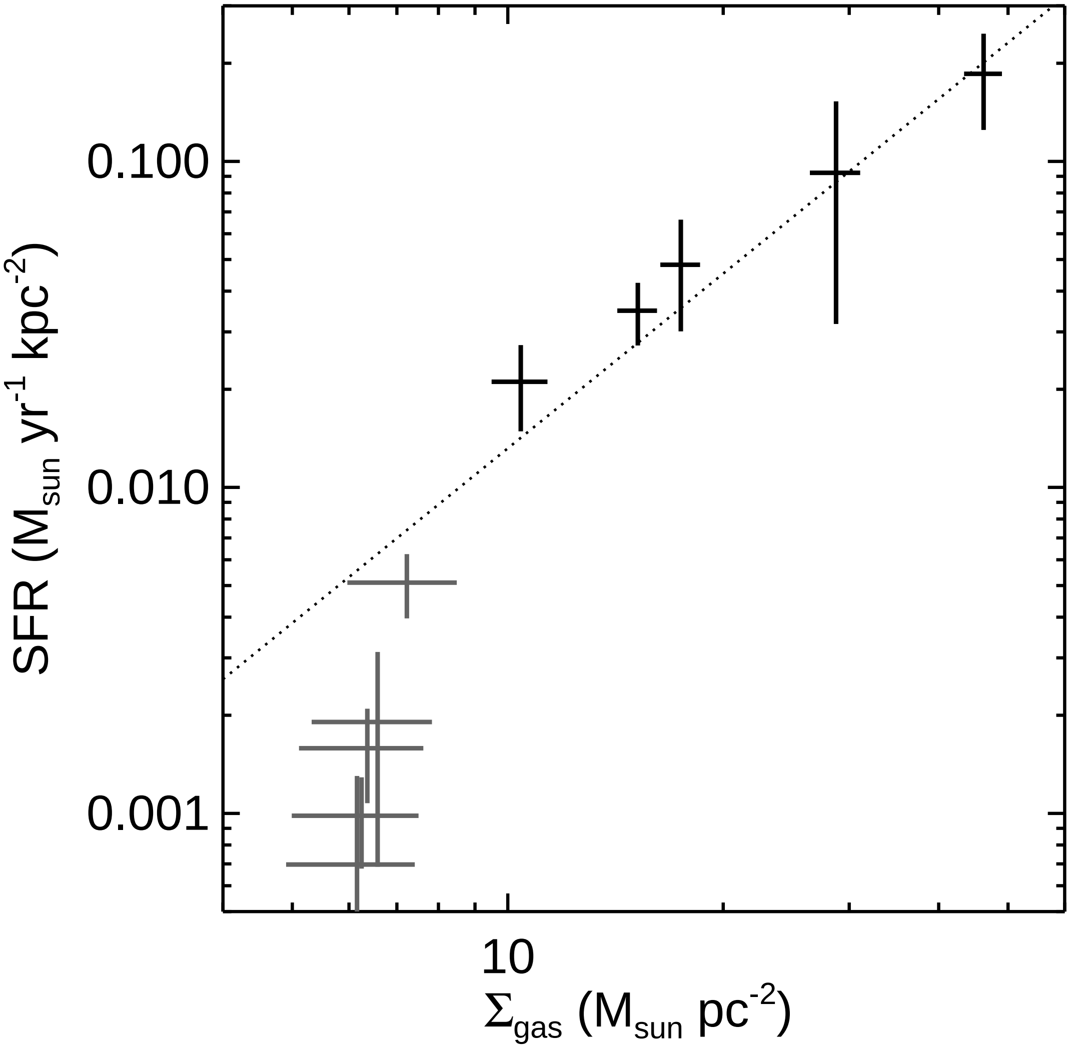

FIG. 14.— The star formation rate surface density (normalized to a Kroupa IMF) at previous epochs (back to 450 Myr ago) from our star formation histories of the INNER-1 (inside the disk break; black) and INNER-2 (outside the disk break; gray) regions vs. the gas surface density during those epochs (taken from the left panel of Figure 13). Within a given region, our assumptions force the density to increase farther into the past (see § 4.2). Therefore higher densities represent earlier epochs, back to 450 Myr ago with the same time resolution as the left panel of Figure 13. The dotted line shows the star formation law for $\Sigma_{\rm HI}$ in NGC 2976 from taken directly from Bigiel et al. (2008). Correcting their relation to Σ_{gas} would shift the dotted line to the right. In general, there is good agreement with the slope for gas densities >7 $M_\odot$ pc^{-2}. The reduction in star formation efficiency below 7 $M_\odot$ pc^{-2} is comparable to what is seen in other dwarf galaxies, but steeper than found in THINGS for NGC 2976.